Heliyon 9 (2023) e21345

Contents lists available at ScienceDirect

Heliyon

journal homepage: www.cell.com/heliyon

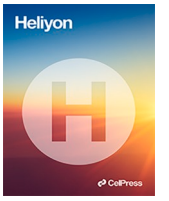

# Performance evaluation of a flighted rotary dryer for lateritic ore in concurrent configuration

Armando Rojas Vargas [a,b,**], Liudmila Pérez García [c], Crispin Sánchez Guillen [d], Forat Yasir AlJaberi [e,***], Ali Dawood Salman [f,*], Saja Mohsen Alardhi [g], Phuoc-Cuong Le [h]

[a] Industrial Engineering Department, Universidad of Holguín, Cuba
[b] Empresa de Servicios Técnicos de Computación, Comunicaciones y Electrónica "Rafael Fausto Orejón Forment", Holguín, Cuba
[c] Chemical Engineering Department, University of Oriente, Santiago de Cuba, Cuba
[d] Centro de Investigaciones Del Níquel "Alberto Fernández Monte de Oca", Holguín, Cuba
[e] Chemical Engineering Department, College of Engineering, Al-Muthanna University, Al-Muthanna, Iraq
[f] Department of Chemical and Petroleum Refining Engineering, College of Oil and Gas Engineering, Basra University for Oil and Gas, Basra, Iraq
[g] Nanotechnology and Advanced Material Research Center, University of Technology, Iraq
[h] The University of Danang-University of Science and Technology, Danang 550000, Viet Nam

ARTICLE INFO

*Keywords:*
Rotary dryer
Residence time
Black box model
Mathematical modelling
Simulation

ABSTRACT

The lateritic ore drying in the Cuban nickel producing industry is realized within flighted rotary dryers. In this investigation, performance indicators in regards to transfer of momentum, heat and mass were evaluated. The dryers operate in a concurrent configuration with combustion gas, at a productivity between 40 t $h^{-1}$ and 50 t $h^{-1}$. The distribution function of the residence time (RTD) was best fitted to a model of a multi-branch tanks-in-series system, theoretical residence time was 51 ± 2 min and experimental mean residence time 61 min, at a rate of 45 t $h^{-1}$ and hydraulic efficiency 1.23, due to the presence of dead-zoon. Mass and energy balance was made following a "black box" model, as results, the specific fuel consumption was 27.25 ± 0.25 kg fuel $t^{-1}$ of wet ore, specific energy consumption 79.66 ± 0.95 kg fuel $t^{-1}$ of $H_2O$ evaporated, energy efficiency 97.28 ± 0.01 %, thermal efficiency 66.88 ± 0.71 % and drying efficiency 98.77 ± 0.12 %. Mathematical modelling was made using a system of differential equations, the rate of drying in falling rate period was estimated by Arrhenius equation, then, temperature profile and ore moisture content along the dryer was simulated. The model provided a successful predictive performance; for an inlet gas temperature between 850 °C and 900 °C, the ore moisture was reduced form 33.0 % (wet basis) to a range depending on the dryer productivity, from 3.0 % to 7.1 %. Designing a computerized system that implements these algorithms can benefit on efficiency and productivity of the production plant.

* Corresponding author.
** Corresponding author. Industrial Engineering Department, Universidad of Holguín, Cuba
*** Corresponding author.
*E-mail addresses:* arojas@eros.moa.minem.cu (A.R. Vargas), furat_yasir@yahoo.com (F.Y. AlJaberi), ali.dawood@buog.edu.iq (A.D. Salman).

https://doi.org/10.1016/j.heliyon.2023.e21345
Received 2 August 2023; Received in revised form 6 October 2023; Accepted 19 October 2023
Available online 30 October 2023

## 1. Introduction

Flighted roraty dryer are used in a variety of industrial process to processing granular or particulate materials. This dryer involves a long cylindrical drum inclined slightly with respect to the horizontal plane, towards the effluent, and it is constructed internally with an array of flights along the drum's length. The drying gas is introduced as countercurrent or concurrent to the flow of solid [1–3].

The operation of the rotary dryer is known as a complex process gas-solid, this involves simultaneous and interdependent mass and heat transfer among the products and the drying gas, as well as the transport of both phases throughout the dryer [4,5].

Momentum transfer in a rotary drum contains the movement of particles in the transverse plane perpendicular to the drum-axis, and toward the axial direction. These are generally investigated in terms of solids' holdup throughout the drum and residence time distribution, respectively. As the dryer rotates around its particular axis, solids are picked up by the action of flights, lifted for a certain distance around the drum periphery and then, fall via the gas-stream in a cascading curtain, the particle bouncing, rolling and sliding on influence with the dryer's bottom [6].

The total holdup throughout a dryer is denoted by the sum of both the active (air-borne) holdup (AH) and the total passive (TP) holdup. According to Ref. [7] mechanistic model, the solids within the drum into the phase air - borne contain the particles falling from the flights under the action of gravitational, frictional, and centrifugal forces. The drum-borne and flight-borne contain the particles that still in the drum base and the flights, respectivally, witch are the total passive holdup (Fig. 1).

The flights promote contact among solids and the drying gas as well as influencing the residence time of solids throughout the dryer. When the flights are not filled to their designed capacity, the dryer is designated as an under-loaded operating and the flight occurs ***after*** 9 o'clock positions, thus the particles' residence time in the active region is shorter compared to the period needed for an effective drying. On the other hand, a design over-loaded dryer is when more solids fill the flights more than required, this occurs *before* the positions of the 9 o'clock and the excess of solid rolls in the dryer's base; therefore, results into reasonable lower efficiency of the dryer. The operation's point with a maximum interaction gas-solid is a design loaded of such dryer in which the fights are at the maximum capacity and occurs *at* the 9 o'clock positions [6,8–10].

Several geometric parameters of flighted rotating dryer have been formulated to optimize the gas-solid contact. The dynamic angle of repose (Θ, rad) is formed by the bed material to the horizontal; in contrast to that, kinetic angle of repose (γ, rad) is conceived by solid content in the fight with the horizontal, almost depends on the fight's circumferential-position or discharge angle (δ, rad). Final discharge angle ($\delta_L$, rad) is the angular-position of the flight where the last particles leave the flight sheet [3,11,12] (Fig. 2).

The final discharge angle ($\delta_L$) determine the amount of particles and its distribution in the air-borne phase, this increase with the flight length ratio ($s_2/s_1$), the rotational speed (n) and drum diameter. When the repose kinetic angle of the particle bed is attained ($\alpha = \gamma$), the final discharge of solids proceed [3,8].

[6] used the 9 o′clock positions to define limits of the loading capacity (design loaded dryer) in a horizontal-pilot scale flighted rotary dryer, two-segment flights. The mass of air-borne solid was determined performing a combination of image-analysis calculations and Eulerian–Eulerian Computational Fluid Dynamics (CFD) simulation. As the rotational speed (n) increased from 2.5 to 4.5 rpm leads to an increase in the dynamic angle of repose (Θ) form 44.7° to 62.3°, the bulk density of the flight-borne solids, and the solids' discharge rate into the airborne phase which increased the holdup of the total dryer.

Likewise [12], investigated the effect occurred by angulations in two-segment flights on the particle dynamics by methods

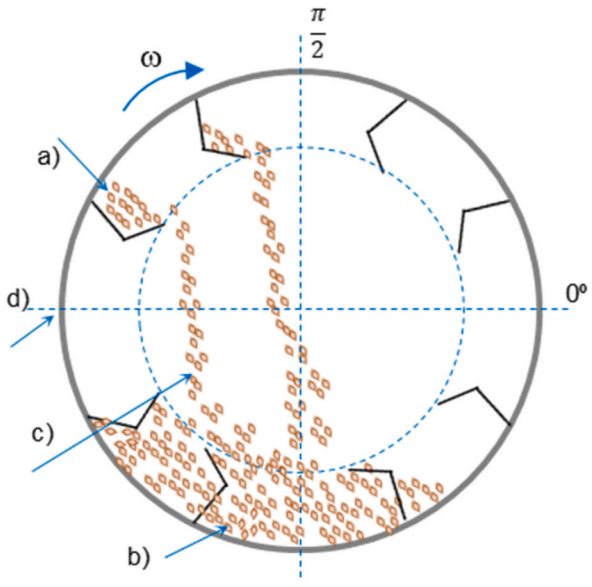


**Fig. 1.** Total holdup in a flighted rotary drum, a) Flight-borne holdup (passive), b) Drum-borne holdup (passive), c) Air-borne holdup (active), d) 9 o′clock positions.

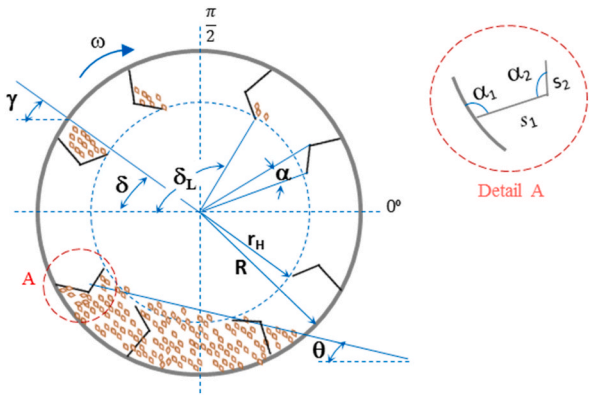


**Fig. 2.** Geometrical parameters of flighted rotary drum: R [m] drum radio, $r_H$ [m] effective radial distance, γ [rad] kinetic angle of repose, δ [rad] flight's discharge angle, $\delta_L$ [rad] final discharge angle, Θ [rad] dynamic angle of repose, $s_1$ and $s_2$ [m] two-segment flights length, $\alpha_1$ and $\alpha_2$ [rad] angulations in flights.

experimental and numerical simulation at 21.3 rpm (Fr = 0.027), the best configurations that intensified the contact solid - fluid were $100^\circ \leq \alpha_2 \leq 110^\circ$ at $\alpha_1 = 90^\circ$ (Fig. 2). For its part [3], documented a mathematical model for evaluating the final discharge angle ($\delta_L$, rad) of rectangular-flights to scale-up the flight design, a highly significant agreement was attained between the experimental observations and the predictions with the model.

On the other hand, momentum transfer in a rotary dryer was studied in terms of (RTD) of solid particles within dryer. RTD is the probability distribution function of numerous values of time that fluid elements discharge a known continuous system (or semi-continuous), of one or more unit operations [13].

Drum diameter (D), length (L), cylinder tild angle (λ), number of rotations per minute (n); the arrangement, shape and number of flights ($n_f$) of particle, as well as the angle of repose are decisive factors for the RTD and therefore, for the efficiency of a rotary dryer. The following ranges are proposed: $3 < L/D < 10$, $2^\circ < \lambda < 5^\circ$, $2 < n < 10$ rpm [1]. Likewise [14], proposed the range $5 < n_f/D < 10$ and [15] about $7 < n_f/D < 10$. The proportion of air-borne to flight-borne solids is reported between 10 % and 15 % of the total holdup [6,9,10].

The most applied models on the RTD measurement in rotary dryer, in a significant agreement with the data set are: tank in series model, axial dispersion model, and modified Cholette-Cloutier's. This last model considers the presence of dead-spaces, that is a non-ideal behavior of the solids transportation, which can lead to improvements in dryer design the dryer design [4,16–19]. The literature showed the absence of comprehensive experimental works covering nickel laterite ore.

In addition, several published works dealing with mathematical modelling of rotary dryer to predict the temperature and moisture profiles of phases, solid and gas, within the dryer. These models are different in the mathematical expression of drying rate, equilibrium moisture and heat transfer; particle chemical-physical properties; the residence time distribution; and the operating parameters: flow, temperature and moisture [1,2,9,16,20–23].

[24] presented a phenomenological model in stationary state for nickel laterite ore drying in a rotary cylindrical kiln on a semi-industrial scale; and [25] obtained a drying kinetics model of a nickeliferous limonitic laterite ore using a thermogravimetric technique. However, it is necessary identifying the specific models best explicative for the ore drying in the industrial installation.

Starting of modelling and simulation of mass and heat transfer in rotary dryer, some performance indicators have been reported relating with thermal, energy, exergetic and drying efficiency; and specific consumption of energy [26–28]. These indicators are used to compare the results with those of the industrial process; also, these are base criteria for the application of technological improvements such as: new energy sources, models, design modifications, and optimization of control parameters.

Therefore, the aim of this study was to estimate performance indicators on the lateritic ore drying within flighted rotary dryer at the nickel producing industry in Cuba. These indicators are correlated to momentum, mass and heat transfer.

For this, ore transport model within the rotary dryer was determined by numerical modelling of the (RTD), and then, some performance indicators of momentum transfer were evaluated in regards to deviations from ideal flow. In particular, was included [29]; which was previously applied to test the mixer's RTD [13,30].

Furthermore, a "black box" model was performed to carry out the mass and energy balance, and determining the fuel flow, primary and secondary air, and the chemical composition of dryer gas at the inlet and outlet of rotary drum; which allowed specifying performance indicators in terms of efficiency and productivity.

Eventually, mathematical modelling of dryer was made to estimate the impact of some input variables on the drying performance, and the most suitable input variables to change the output were determined using the approach develop by Ref. [16]. The mathematical model identified consists of a system of four differential equations presented by Refs. [2,9,21,31]. Furthermore, this include the drying rate model in period of the falling rate by Arrhenius equation with the constants presented by Ref. [25], and equilibrium moisture model performed from the date presented by Ref. [32]. The volumetric heat transfer coefficient was evaluated by the Perry' model [33], and heat loss coefficient by the Arruda's model [34].

Then, for the models validation, numerical simulation results were compared with the mass and energy balance, the analysis of

predictive performance, the insight and explain of industrial operation and the literature.

In the lateritic ore processing industry for nickel production in Cuba, the ore preparation stages consist of the following operations: Natural drying by arranging the ore in piles and exposing the material to the solar radiation; crushing to a fragments size of up to 100 mm; direct contact drying in flighted rotary dryers to a moisture content between 0.04 and 0.05 kg $H_2O$ $kg^{-1}$ of wet solid; and dry grinding to a particle size of up to 83 % of class: 0.074 mm. Subsequently, the ore is provided to reduction furnaces Herreshoff, where nickel is selectively reduced to metallic grade [35].

Moisture content of lateritic ore out-of-specification causes agglutination of the small particles with each other, adhesion and sieves holes covering, consequently change the operation of the classifier [36] and decreases the sieving efficiency. Moisture has an unfavorable effect on the consumption of the specific energy by minimizing the throughput on the comminuting process [37]. Wet fine particles are adhered to the large material in the ore grinders, causing losses in the scalping process of the rocks with size greater than 2 mm. Likewise, the higher the ore moisture, the higher the consumption of fuel in the reduction process.

So, it is expected that the results of this work contribute to provide a better understanding of the drying mechanisms of the Cuban nickel-laterite ore.

## 2. Material and methods

### 2.1. Feed material

The lateritic mineral fed to the rotary dryer had a mean concentration (± standard deviation) of nickel (Ni) 1.1 ± 0.03 %, cobalt (Co) 0.088 ± 0.004 %, iron (Fe) 41.86 ± 1.36 %, magnetic fraction 3.39 ± 0.79 % and particle mean diameter (dp) 0.1688 mm. The mineral number, which is understood as an ore quality, was 0.80 ± 0.36 %, Eq. (1) (Table 1) [38].

$$Nm = \frac{C_{Ni}\, C_{Fe}}{C_{MgO}\, C_{SiO_2}} \tag{1}$$

### 2.2. Drying system of nickel laterite ore

Wet ore is discharged from conveyor belts into ore bins. The feeders dose the load to the passage chamber of the dryers. The productivity of each dryer is between 40 t $h^{-1}$ and 50 t $h^{-1}$ of dry ore (Table 2).

The ore enters the dryer at 30 °C and moisture (x) between 0.32 and 0.34 kg $H_2O$ per kg of wet solid and is placed in contact with hot gases in concurrent configuration. As a result, the ore discharges with moisture of 0.04–0.05 kg $H_2O$ $kg^{-1}$ of wet solid at a temperature of 75–110 °C (Fig. 3).

Each rotary dryer has a combustion chamber to produce the flue gas at 1480 °C. The combustion fan disperses the fuel inside the chamber from 95 to 150 °C, with a pressure of 1.47–1.96 MPa. The fuel consumption rate is 25.65 kg per ton of wet ore. The flue gas come into contact with secondary air to reach the flow required of drying gas; but at the same time the temperature decreases between 700 °C and 750 °C. Then, drying gas is heated in heat exchangers with water steam (0.54 MPa and 128 °C) to reach a temperature ($T_G$) between 800 and 900 °C. Finally, the drying gas enter the rotating cylinder (drum) and transfer heat to the mineral, absorb moisture and discharge between 76 °C and 90 °C. The lateritic ore presents a retention time between 55 and 65 min.

### 2.3. Models development

#### 2.3.1. Ore transport model

A mass of 60 kg of the ($Na_2CO_3$) tracer was introduced at the feed input end using the pulse method in less than 1/30 the theoretical residence time; then, at regular intervals of 5 min, the concentration of the tracer (Ci) in the outlet was observed at the discharge end, Eq. (2) used to determine the RTD function, $E$(t), [13,39,40].

$$E(t) = \frac{C(t)}{\int_0^\infty C(t)\, dt} \cong \frac{(C_i - C_0)_i}{\sum_{i=0}^{n} (C_i \Delta t)} \tag{2}$$

where, $E$(t) [$min^{-1}$].

$\boldsymbol{C_0}$: the initial concentration in mg/L
$\boldsymbol{C_i}$: the concentration after a certain time ($t_i$), in mg/L
$\boldsymbol{C_n}$: the final concentration in mg/L
$\boldsymbol{\Delta t}$: time between which measurements are taken, in min

**Table 1**
Particles size distribution of feed material.

| Dp (mm) | −0.045 | −0.075 + 0.045 | −0.150 + 0.075 | −0.177 + 0.150 | −3.36 + 2.00 | −4.75 + 3.36 | −6.35 + 4.75 |
|---|---|---|---|---|---|---|---|
| % | 80.77 | 4.30 | 4.29 | 7.14 | 2.75 | 0.33 | 0.48 |

**Table 2**
Rotary dryer main dimensions.

| L [m] | D [m] | n [rpm] | λ [m•m$^{-1}$]; [deg.] | Ls [t.h$^{-1}$] | $\tau_0$ [min] |
|---|---|---|---|---|---|
| 39.624 | 4.267 | 2.06–2.16 | 0.04167; 2° 23′ | 40.0–50.0 | 55.0–65.0 |

L: length, D: Drum diameter, n number of rotations per minute, λ: cylinder tild angle.

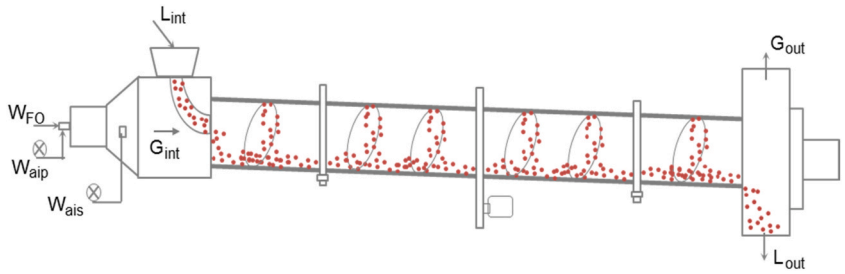


**Fig. 3.** Schematic depiction of the combustion chamber and industrial flighted rotary dryer. L and G are the flows [kg h$^{-1}$] of laterite ore and drying gas, respectively. W [kg h$^{-1}$] is the flow of fuel (FO), primary air (aip), secondary air (ais). Int-inlet, Out-outlet.

A normalized RTD is used to compare flow performance between systems of different sizes, Eq. (3)

$$E(\theta) = E(t)\ t_m \tag{3}$$

where the symbol θ is the ratio of ($t/t_m$) and $E(\theta)$ refers to the normalized RTD function. The symbol $t_m$ is known as the observed mean residence time and defined as the first moment of the RTD, Eq. (4) [13,39,41].

$$t_m = \frac{\int_0^\infty t\ E(t)\ dt}{\int_0^\infty E(t)\ dt} = \int_0^\infty t\ E(t)\ dt \cong \frac{\sum_{i=0}^{n} t_i\ (C_i - C_0)}{\sum_{i=0}^{n} (C_i - C_0)} \tag{4}$$

The second moment is designated as the variance; which refers to the dispersion of the distribution, Eq. (5) [13,42].

$$\sigma^2 = \int_0^\infty (t - t_m)^2\ E(t)\ dt \tag{5}$$

In general, the $t_m$ parameter is equivalent to the theoretical residence time parameter ($t_0$) as long as there are no considerable deviation from the ideal flow.

[15] suggested Eq. (6) for residence time estimation of granular solids in the rotating drums involving dryers and kilns [1,43–46].

$$t_0 = 0.3344 \left(\frac{Z}{D}\right) \frac{n^{-0.9}}{\lambda} + \epsilon\ 0.6085\ Z\ d^{-0.5} \left(\frac{G_s}{L_s}\right) \tag{6}$$

where, $t_0$ is the theoretical residence time in [min], D is the drum internal diameter in [m], Z is the section length in [m], n is the rotation rate of drum in [min$^{-1}$], $\lambda$ is the inclination angle of drum [rd], d is particle diameter [mm], $G_s$ [kg s$^{-1}$] is gas flow, $L_s$ [kg s$^{-1}$] is ore flow. The symbol epsilon ($\epsilon$) is equal to (1) for concurrent, and (−1) for countercurrent flow.

[47] correlated experimental data of a design-loaded shell, by Eq. (7).

$$t_0 = Z\ \frac{0.375}{tan\ \lambda\ n\ D} + \epsilon\ \frac{m}{60}\ u_g \tag{7}$$

[48]proposed Eq. (8) based on a theoretical analysis.

$$t_0 = \frac{Z}{f_H\ n\ D\ \left(tan\ \lambda + \epsilon\ k_m\ u_g\right)} \tag{8}$$

[49], Eq. (9).

$$t_0 = \frac{Z}{a\ tan\ \lambda\ n\ D} \tag{9}$$

[50], Eq. (10).

$$t_0 = Z\,\frac{22.7/60}{\lambda\, n^{0.9}\, D} \tag{10}$$

where m = 177 s $m^{-1}$ is a constant, $f_H$ is the cascade factor varying between (2) and (π), and increasing as solid hold up raises; $k_m$ = 0.001 s $m^{-1}$ is a constant for a given material; $u_g$ [m $s^{-1}$] is the gas-velocity and constant $a$ = 2.4 [-].

Ore transport model within the dryer was determined by numerical modelling of the RTD, considering the following models:

*2.3.1.1. Tanks-in-series.* This model suggests that the flow throughout a vessel could be depicted by the flow through a series of several equal-sized continuous stirred tank reactors (N-CSTR) model, Eq. (11) [13,39–41,51].

$$E(\theta) = \frac{N\,(N\,\theta)^{N-1}}{(N-1)!}\,exp(-N\,\theta) \tag{11}$$

where the symbol *N* is the regulating variable of this model.

Dispersed Plug Flow

Dispersed plug flow model suggests that the fluid moves throughout the system at a constant flow rate, the radial concentration gradient and diffusion radial are neglected. The Peclet-Bodenstein module is emphasized by the vessel dispersion number, Eq. (12) [13, 51]:

$$Bo = \frac{D}{\upsilon\, L} \tag{12}$$

Where: *D*, L, and $\upsilon$ are designated the coefficient of dispersion, the vessel's length or its diameter, and the velocity of electrolyte, respectively.

Based on *Bo* value, the status of dispersion of such designed system could be categorized as follows:

- *Bo* = 0.002: Small or negligible and plug flow behavior of fluid.
- *Bo* = 0.025: Medium and non-ideal flow behavior of fluid.
- *Bo* = 0.2: Large and a complete mixing behavior of fluid.

For *Bo* value less than 0.01, the normalized value of RTD does not pointedly change alter as the electrolyte flows through the measurement point which is given by Eq. (13), and the normalized value of variance indicator is given by Eq. (14).

$$E(\theta) = \frac{1}{2\sqrt{\pi\, Bo}}\,exp\left[-\frac{(1-\theta)^2}{4\, Bo}\right] \tag{13}$$

$$\sigma_\theta^2 = \frac{\sigma^2}{t_m^2} = 2\, Bo \tag{14}$$

Regarding the value of *Bo* is larger than 0.01, for an open-boundary condition where the flow is not influenced by passing through the input and output of the designed system, Eq. (15), and the normalized variance indicator, by Eq. (16) [13,41,52,53].

$$E(\theta) = \frac{1}{2\sqrt{\pi\,\theta\, Bo}}\,exp\left[-\frac{(1-\theta)^2}{4\,\theta\, Bo}\right] \tag{15}$$

$$\sigma_\theta^2 = \frac{\sigma^2}{t_m^2} = 2\, Bo + 8\, Bo^2 \tag{16}$$

*2.3.1.2. Multi-branch tanks-in-series.* This model was proposed by Ref. [29] and conducted to characterize the degree of mixing and estimate the presence of dead-zoon or bypassing in a mixer, Eqs. (17)–(20) [13,30].

$$E(\theta) = C_1\,\theta^{n-1}\,\exp(-n\,\beta\,\theta) + C_2\,\theta^{m-1}\,\exp\left(-m\,\frac{\beta}{\alpha}\,\theta\right) \tag{17}$$

$$C_1 = f\,\frac{n^n}{(n-1)!}\,\beta^n \tag{18}$$

$$C_2 = (1-f)\,\frac{m^n}{(m-1)!}\left(\frac{\beta}{\alpha}\right)^m \tag{19}$$

$$\beta = f + (1-f)\,\alpha \tag{20}$$

where, $\alpha = t_{m2}/t_{m1}$ is characterized as the ratio of the main branch residence time to the side branch residence time; $f$ refers to the

fraction of total fluid flow to a branch which equals *one*; *n* and *m* depicted to the total number of stirred-tanks in branches 1 and 2, respectfully.

*2.3.1.3. Model of perfectly mixed-reactors-in-series with dead-space and bypassing.* RTD function that relates the number of mixed reactors-in-series, dead zoon and bypassing at each mixed-tank was documented by Ref. [54], Eq. (21).

$$E(\theta)=\frac{N\,n}{M}\sum_{i=1}^{N}\frac{N!\;exp\left(-\frac{n\,N\,\theta}{M}\right)\left(\frac{n\,N\,\theta}{M}\right)^{i-1}(1-n)^{N-i}\,n^{i}}{(N-i)!\;i!\;(i-1)!}+(1-n)\;\delta\left(\frac{n\,N\,\theta}{M}\right) \tag{21}$$

where, *N* is the number of (CFSTR) reactors, allowing for fractions of dead-zoon and bypassing equal (1-M) and (1-n), respectively, at each CFSTR.

Average Relative Error (*ARE*) and Marquardt's Percent Standard Deviation (*MPSD*) are performed to verify the consistency of RTD models, Eqs. (22) and (23) respectively.

$$ARE=\frac{1}{n}\sum_{i=1}^{n}\left[\left(\frac{E(\theta)_{exp}-E(\theta)_{model}}{E(\theta)_{exp}}\right)\right] \tag{22}$$

$$MPSD=\sqrt{\frac{1}{n-P}\sum_{i=1}^{n}\left[\left(\frac{E(\theta)_{exp}-E(\theta)_{model}}{E(\theta)_{exp}}\right)\right]^{2}} \tag{23}$$

where, *n* and *P* are the numbers of data points and parameters, respectively.

### 2.3.2. Black box model

The "Black box" model represents the input-output relationships of the drying system; but in this case clues are showed about its inner workings for a much easier understanding and interpretation of the physicochemical transformations of materials. The model was used in the trial-and-error process, to estimate operation parameters and then compare the results with the target values (Fig. 4).

The combined balance of mass and energy in concurrent configuration was performed by the "black box" model, Eqs. (24) and (25) [55].

$$Gs\left(Y_{s,out}-Y_{s,int}\right)=Ls\left(X_{s,int}-X_{s,out}\right) \tag{24}$$

$$Ls\,H_{L,int}+Gs\,H_{G,int}=Ls\,H_{L,out}+Gs\,H_{G,out}+Q_{p} \tag{25}$$

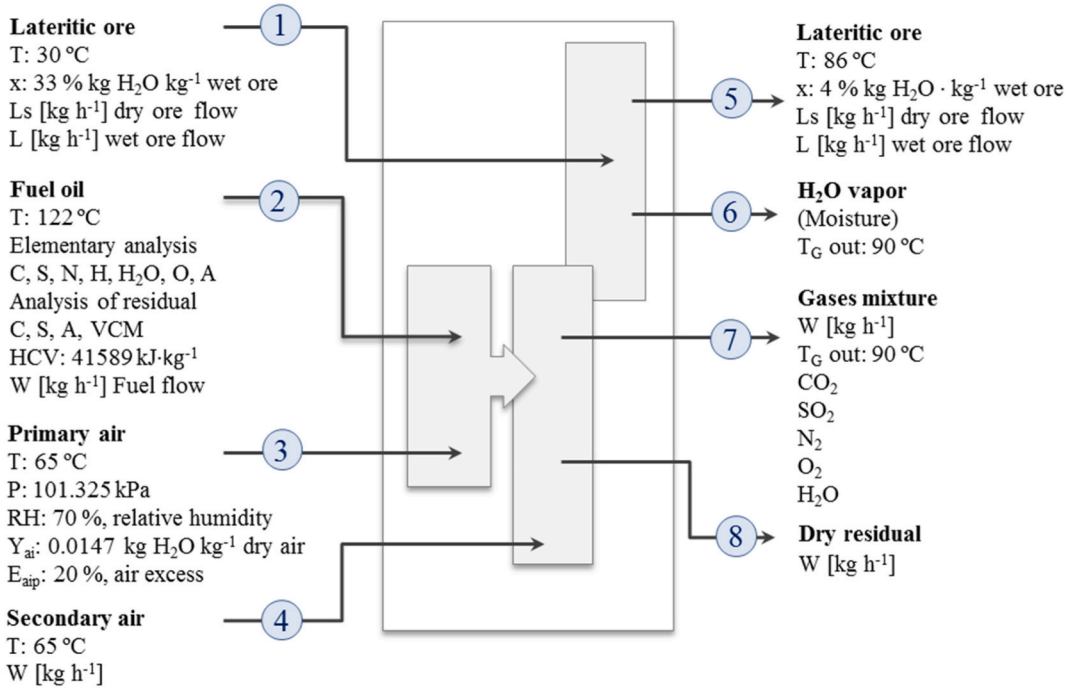


**Fig. 4.** Representation of "Black box" model.

where, $Gs$ [kg $h^{-1}$] is the flow of dry gas, $Ls$ [kg $h^{-1}$] is the dry solid flow, $Xs$ [kg $H_2O$ $kg^{-1}$] dry solid is the solid moisture, $Ys$ [kg $H_2O$ $kg^{-1}$] dry gas is gas moisture, $Q_p$ [kJ] is the lost heat, $H_L$ [kJ $kg^{-1}$ dry solid] is the enthalpy of the solid, $H_G$ [kJ $kg^{-1}$ dry gas] is the enthalpy of the gas.

Moisture wet basis (x) and (y) is converted to dry basis (X) and (Y) by Eqs. (26) and (27), respectively.

$$X = \frac{x}{1-x};\ \frac{kg\ H_2O}{kg\ dry\ solid} \tag{26}$$

$$Y = \frac{y}{1-y};\ \frac{kg\ H_2O}{kg\ dry\ gas} \tag{27}$$

The enthalpy of solid and gas was determined by Eqs. (28) and (29), respectively [55].

$$H_L = (T_L - T_R)\ (Cp_{Ls} + X_s\ Cp_w) \tag{28}$$

$$H_G = Cp_{Gs}\ (T_G - T_R) + Y_s\ \lambda_0 \tag{29}$$

where, $Cp_{LS}$ [kJ (kg °C)$^{-1}$] is the specific heat of dry solid, $Cp_w$ [kJ (kg °C)$^{-1}$] is the specific heat capacity of liquid water that accompanies the solid, $T_R$ [°C] is the reference temperature, $Cp_{GS}$ [kJ (kg °C)$^{-1}$] specific heat of dry gas.

The specific heat of lateritic ore was determined by Eq. (30) form 20 °C to 100 °C [56] and latent heat of vaporization of water by Eq. (31).

$$Cp_L = 0.465185294117647 + 0.00450005 \quad T_L \tag{30}$$

$$\lambda_w = \frac{R}{M_w}\ [6547.1 - 4.23\ (T + 273.16)] \tag{31}$$

Where, $\lambda_w$ [kJ $kg^{-1}$], $R = 8.3145$ kJ $kmol^{-1}$ $K^{-1}$ is the universal gas constant, $M_w = 18.01$ kg $kmol^{-1}$ is the molar mass of water, $T$ [°C] is the temperature.

The primary air flow fed to the combustion chamber was determined by Eq. (32)–(35), from fuel elemental analysis (Table 3) [57]:

$$W_{aip} = (W'_{O_2} + W_{N_2} + W_{H_2O})\left(1 + \frac{E_{aip}}{100}\right) \tag{32}$$

$$W'_{O_2} = \frac{8}{3}\ C + 8\ H - O + S \tag{33}$$

$$W'_{N_2} = W'_{O_2}\ \frac{0.768}{0.232} \tag{34}$$

$$W'_{H_2O} = Y\ (W'_{O_2} + W_{N_2}) \tag{35}$$

where, $W_{aip}$ [kg $kg^{-1}$] is the primary air flow per kg fuel, $E_{aip}$ [%] is the percent of excess primary air equal to 20 %, $W'$ [kg $kg^{-1}$] is the of stoichiometric flow of oxygen ($O_2$), nitrogen ($N_2$) and water ($H_2O$).

Outlet gas flow from the combustion chamber was determined by Eq. (36)–(41):

$$W_{CG} = W_{CO_2} + W_{SO_2} + W_{N_2} + W_{O_2} + W_{H_2O} \tag{36}$$

$$W_{CO_2} = \left(C - \frac{A}{A_r}\ C_r\right)\ \frac{44}{12} \tag{37}$$

$$W_{SO_2} = \left(S - \frac{A}{A_r}\ S_r\right)\ \frac{64}{32} \tag{38}$$

$$W_{N_2} = \left(N + W_{O_2}\ \frac{0.768}{0.232}\right)\left(1 + \frac{E_{aip}}{100}\right) \tag{39}$$

**Table 3**
Fuel elemental analysis.

| Elemental analysis [%w] | | | | | | | Residue analysis [%w] | | | | API | *VCS* [kJ.kg$^{-1}$] |
|---|---|---|---|---|---|---|---|---|---|---|---|---|
| C | S | N | H | $H_2O$ | O | A | $C_r$ | $S_r$ | $A_r$ | VCM | | |
| 63.70 | 2.50 | 0.08 | 11.85 | 0.40 | 0.62 | 0.05 | 0 | 0 | 100 | 0 | 13.70 | 41589 |

$$W_{O_2} = \frac{E_{aip}}{100}\, W'_{O_2} \tag{40}$$

$$W_{H_2O} = H\,\frac{18}{2} + Y\, W'_{O_2}\left(1+\frac{0.768}{0.232}\right)\left(1+\frac{E_{aip}}{100}\right) \tag{41}$$

where, $W_{CG}$ [kg kg$^{-1}$] is the flue gas flow per kg fuel and the elements of Table 3 in mass fraction.

Secondary air flow was calculated as the difference between the wet gas feed by Eq. (24) and the combustion gas flow by Eq. (36) (Fig. 4).

The energy balance in the combustion chamber – rotary dryer system was carried out according to "black box" model, Fig. 4, by Eq. (42)–(50) [57].

Energy entered into the system ($Q_0$, kW)

$$Q_0 = W_2\, HCV \tag{42}$$

where, HCV [kJ kg$^{-1}$] is the higher calorific value.

Energy consumption for ore moisture evaporation ($Q_{11}$, kW)

$$Q_{11} = (H_{w5} - H_{w1} + \lambda_w)\, Ls\, (X_{s1} - X_{s5}) \tag{43}$$

where, $H_{w5}$ [kJ kg$^{-1}$] is the $H_2O$ enthalpy at 0.101325 MPa and 88 °C, $H_{w1}$ [kJ kg$^{-1}$] is the $H_2O$ enthalpy at 0.101325 MPa and 30 °C [58], $\lambda_w$ at 88 °C.

Energy consumption for ore heating ($Q_{12}$, kW)

$$Q_{12} = (Cp_{Ls}\, Ls + Cp_w\, Ls\, X_{s5})\, (T_5 - T_1) \tag{44}$$

Energy consumption for water evaporation that contains the fuel ($Q_2$, kW)

$$Q_2 = 4.1867\, H_2O\, (595.4 + 0.46\, T_7 - T_3)\, W_3 \tag{45}$$

Energy consumption for water formation by the hydrogen combustion of fuel ($Q_3$, kW)

$$Q_3 = 9\, H\, [4.1867\, (0.46\, T_7 - T_3)]\, W_3 \tag{46}$$

Energy consumption for water evaporation that contain the primary combustion air ($Q_4$, kW)

$$Q_4 = W'_{O_2}\left(1+\frac{0.768}{0.232}\right) Y_{ai}\, 1.925\, (T_7 - T_2)\, W_3 \tag{47}$$

Energy consumption for heating the secondary dry air to chamber temperature ($T_c$) of 850 °C ($Q_5$, kW)

$$Q_5 = W_{ai-s}\, \overline{cp}_s\, (T_c - T_4)\, W_3 \tag{48}$$

Energy consumption for water evaporation that contain the secondary air ($Q_6$, kW)

$$Q_6 = W_{ai-s}\, Y_{ai}\, 1.925\, (T_7 - T_4)\, W_3 \tag{49}$$

Energy lost by the contained heat in the dry gaseous products of combustion that leave the system ($Q_7$, kW)

$$Q_7 = Gs_7\, \overline{cp}_s\, (T_7 - T_2)\, W_3 \tag{50}$$

Energy lost by incomplete combustion ($Q_8 = 0$).

Energy lost by carbon non burnt ($Q_9 = 0$).

First, the heat loss was assumed for a conservative relative error (ξ) in the heat balance; subsequently, the mean value of the losses

**Table 4**
Constants of specific heat versus temperature between 300 K and 2000 K (Eq. (30)).

| Substance | Range T [K] | $c_0$ | $c_1 \bullet 10^{-3}$ | $c_2 \bullet 10^{-6}$ | $c_3 \bullet 10^{-9}$ | $c_4 \bullet 10^{-14}$ | $c_5 \bullet 10^{-18}$ | $c_6$ |
|---|---|---|---|---|---|---|---|---|
| Combustion gas | | | | | | | | |
| $CO_2$ | 375–1300 | −0.11819 | 3.2033 | −4.1611 | 3.4052 | −0.0156 | 0.30046 | 5.21188 |
| $SO_2$ | 375–1300 | 0.40280 | 90.5370 | −59.5470 | 13.4530 | 1590.0 | −29974.0 | −0.00011 |
| $N_2$ | 375–2000 | 1.0385 | −61.690 | 1.6358 | −1.3755 | 0.5181 | −0.74335 | 1.31594 |
| $O_2$ | 375–2000 | −0.54009 | 2.6849 | −2.5707 | 1.4075 | −0.4076 | 0.48923 | 14.76330 |
| Mixture[a] | 375–1300 | 0.67392 | 27.9250 | 0.4052 | −0.4713 | 0.1708 | −0.18762 | 3.84716 |
| Water | | | | | | | | |
| State | Range T [K] | $c_0$ | $c_1 \bullet 10^{-2}$ | $c_2 \bullet 10^{-4}$ | $c_3 \bullet 10^{-7}$ | $c_4 \bullet 10^{-10}$ | $c_5 \bullet 10^{-14}$ | $c_6$ |
| $H_2O$ liquid | 273–573 | −27.4041 | 41.5297 | −21.5970 | 0.5558 | −0.7098 | 0.036236 | 0.0 |
| $H_2O$ vapor | 300–2000 | 3.3381 | −0.3137 | 442.9240 | −236.60 | 5180.55 | −3005.39 | −15.2939 |

[a] Mixture of flue gases and secondary air.

in the control volumes (dz) was determined by Aruda′s model, Eq. (57), ξ was calculated and reasonably incorporated into the iterative mass and heat balance process.

Specific heat versus temperature between 300 K and 2000 K was estimated by Eq. (51). The function was obtained from the data set presented by Ref. [33] (Table 4).

$$Cp_G = c_0 + c_1\, T_G + c_2\, T_G^2 + c_3\, T_G^3 + c_4\, T_G^4 + c_5\, T_G^5 + c_6\, T_G^{-0.5} \tag{51}$$

where, Cp [kJ (kg K)$^{-1}$] is the specific heat capacity, $T_G$ [K] is the gas temperature.

### 2.3.3. Mathematical model

The mathematical model was predicted based on the application of energy and mass conservation equations on the phases gas (G) and the particles solid (L). The following assumptions were made [2,9,21]:

- The flow model through the dryer is Plug flow.
- The operating is at concurrent flow and at stationary state on a control volume of dryer (dz).
- The ore particles possess a spherical geometry and their dimensions still constant.
- The reference temperature and pressure are constants.
- The principles of the ideal gas mixture are conducted for gases in the system.
- The composition of gases in the combustion chamber is constant for each ore flow.
- The heat capacities of materials drying gas and lateritic ore are depending on the temperature profile through the dryer.
- The drying process occur in the falling rate period according to Arrhenius equation.
- The potential energy, kinetic energy and exergy of materials are negligible.

Mass balances in a control volume, Eq. (52) and (53).

$$\frac{dX}{dz} = -\frac{R\,M}{Ls} \tag{52}$$

$$\frac{dY}{dz} = \frac{R\,M}{G} \tag{53}$$

Energy balance in a control volume, Eq. (54) and (55).

$$\frac{dT_L}{dz} = \frac{U.\,V\,(T_G - T_L) - \lambda_w\, M\, R}{Ls\,(Cp_L + X\,Cp_w)} \tag{54}$$

$$\frac{dT_G}{dz} = \frac{-U.\,V\,(T_G - T_L) - Cp_G\, R\, M\,(T_G - T_L) - U_p\, A\,(T_G - T_R)}{G\,(Cp_G + Y\,Cp_w)} \tag{55}$$

where, M [kg] is the rate product of solid flow (Ls) and the average residence time ($t_0$), R [kg] water kg$^{-1}$ dry solid s$^{-1}$ is the dryer rate, U [kW (m$^2$ °C)$^{-1}$] is the global coefficient of the volumetric heat transfer, $U_p$ [kW (m$^2$ °C)$^{-1}$] is the coefficient of heat loss, V [m$^3$] and A [m$^2$] are the dryer volume and area respectively.

Volumetric heat transfer coefficient in rotary dryer was estimated by Eq. (56) [33]. This model was as consistent with spectated results as Luikov′s model, cited by Ref. [1], for a fraction of drum cross-section occupied by solids 0.044 (Table 5).

On the other hand, the heat loss coefficient U [kWm$^{-3}$ K$^{-1}$] was determined by Eq. (57) [34].

$$U = 0.237\,\frac{\left(G_s'\right)^{0.67}}{D} \tag{56}$$

$$U_p = 0.022\,\left(G_s'\right)^{0.879} \tag{57}$$

where, $G_s'$ [kg m$^{-2}$ s$^{-1}$] is designated as the mass velocity of dry gas.

The drying rate (K) in the period of the falling rate was assumed by Eq. (58); but K is equal to zero at the equilibrium moisture (X*), then, Eq. (59) was deduced [21].

$$-\frac{dx}{dt} = K = AX + B \tag{58}$$

**Table 5**
Volumetric heat transfer coefficient in rotary dryer by some models at $G_s'$ 1.620 kg m$^{-2}$ s$^{-1}$, $L_s'$ 1.285 kg m$^{-2}$ s$^{-1}$.

| Variable | Unit | Perry model | Luikov′s model | | Agustini model | Aruda model |
|---|---|---|---|---|---|---|
| $f_v$ | % | – | 3.83 | 4.40 | – | – |
| $U$ | kW m$^{-3}$ K$^{-1}$ | 0.0930 | 0.0866 | 0.0933 | 0.0865 | 0.0519 |

$$K = k\ (X - X^*) \tag{59}$$

The Arrhenius equation is extremely correlated to the temperature of the drying gas Eq. (60).

$$k = k_0\ exp\left(-\frac{Ea}{R\ T_G}\right) \tag{60}$$

where $k$, $k_0$, and $Ea$ are designated as the rate constant, frequency constant, and the activation energy in [kJ $mol^{-1}$], respectively. $R$ = 8.3145 kJ $kmol^{-1}$ $K^{-1}$ is the universal gas constant, $T_G$ [K] is the gas temperature.

It was assumed at temperatures below 100 °C, $k_0 = 2.016 \times 10^{-9}$ and $Ea$ = 25.5 kJ $mol^{-1}$, while at higher temperatures $k_0$ = 0.0015 and $Ea$ = 12.90 kJ $mol^{-1}$ [25].

The equilibrium moisture content was determined depending of solid temperature, from date presented by Ref. [32], Eq. (61).

$$X^* = 22.438\ T_L^{-1.453} \tag{61}$$

where, $X^*$ [kg $kg^{-1}$] dried solid is the equilibrium moisture, $T_L$ [°C] is the solid temperature.

Equations of the predicted model were solved using the Euler method with integration step h = 0.05 m. The properties of drying gas and solid were calculated for each control volume (Table 4). Initial conditions are presented in Table 5. The predicted model was validated by comparing the numerical simulation findings with mass and energy balance, the analysis of predictive performance, the insight and explanation of industrial operation and the literature.

#### 2.3.4. Input parameters

Input parameters for laterite ore drying are summarized in Table 6.

### 2.4. Sensitivity analysis

The most suitable input variables (manipulated variable or decision variables) was identified for different operation condition, by estimating the relative index of the output variable (controlled variable) to variations in the input variable. Manipulated variable could be adjusted in order to maintain the controlled variable, i.e. output variable, at its set-value [18,59], Eq. (62).

$$\eta = \frac{(\psi - \psi_{ref})/\psi_{ref}}{(\chi - \chi_{ref})/\chi_{ref}} \tag{62}$$

where, $\eta$ is the relative-index, $\psi$ and $\psi_{ref}$ are the variables' values after and before each change, respectively, $\chi$ and $\chi_{ref}$ are the new and initial values of the input variable, respectively.

### 2.5. Chemical analysis

Atomic absorption spectrophotometry was employed to measure the concentration of metals using a SP-9 Spectrophotometer. All inorganic chemicals performed ($HNO_3$, HCl, $H_3BO_3$, $KClO_3$) were at analytical grade and reagents have been prepared using deionized water.

## 3. Results and discussion

### 3.1. Performance indicators of momentum transfer

The sodium carbonate tracer substance was simultaneously monitored in the effluent of three rotary dryers every 5 min in the industrial process. The operation variables were controlled at its set value by means of the Cuban Supervisory Control and Data Acquisition (SCADA) EROS.

**Table 6**
Input parameters for laterite ore drying.

| Variable | Stream [a] | Code | Unit | Value | Range |
|---|---|---|---|---|---|
| Inlet dry ore flow | 1 | $Ls_1$ | kg•$h^{-1}$ | 4500 | 4000–5000 |
| Inlet ore moisture | 1 | $X_1$ | kg $H_2O$ $kg^{-1}$ wet solid | 0.33 | 22–36 |
| Outlet ore moisture | 5 | $X_2$ | kg $H_2O$ $kg^{-1}$ wet solid | 0.04 | |
| Inlet ore temperature | 1 | $T_{L1}$ | °C | 33 | |
| Outlet ore temperature | 5 | $T_{L2}$ | °C | 80 | |
| Primary air temperature | 3 | $T_{ai\text{-}p}$ | °C | 65 | |
| Secondary air temperature | 4 | $T_{ai\text{-}s}$ | °C | 65 | |
| Outlet gas temperature | 6,7 | $T_{G2}$ | °C | 88 | |

[a] Black box model.

The measurements of Residence Time Distribution (RTD) were trunked at a final time of 120 min, which represents 2.4 times the theoretical residence time ($t_0$) predicted; but a pick of sodium concentration was obtained at the exit age distributions, thus, second moment RTD may results higher and the quality-of-fit of the solid transport model lower than expected. Normalized RTD was determined by Eq. (3); this suggested a behavior different of solid motion through the dryers, which is discussed as follow (Fig. 5).

Some approached were applied to predict the theoretical residence time ($t_0$) and also to compare the quality of estimations, resulting an average values (± standard deviation) of 51 ± 2 min for a drying gas flow ($G_s$) 15.8 kg $s^{-1}$ and dry ore ($L_s$) 12.5 kg $s^{-1}$. All equations presented reasonable predictions due to these include the dryer geometry and flow properties (Table 7).

In the dryers D-2 and D-3, a hydraulic efficiency ($k_0$) < 1 (Table 8) and concentration fluctuations (picks) between 80 and 120 min (Fig. 5) suggests the effect of short-circuit (bypass or channelization). In addition, the tracer ($Na^+$) appeared quickly in the outlet ($5 < t_a < 10$ min), $k_1 = 0.2 < 0.3$; and the period in which 50 % of the tracer ($Na^+$) left the dryer was $k_2 = 0.92 < 1$ [13,60]. This can be the result of deviations from flights design specifications caused by maintenance activity, or breakage of some flights section due to the abrasive effect of the solid; so ore fractions pass faster through the dryer resulting in a lower value of the residence time. Consequently, the energy efficiency and product moisture content is affected.

However, in the rotary dryer D-1, the ($t_m$) was greater than the ($t_0$) and the hydraulic efficiency of $k_0$ is greater than 1; also, after 80 min a second pick was performed, this can be a result of dead-spaces [61] and so, fluids fraction flow toward the effluent stream at a slower velocity compared to the main stream (Fig. 5).

Although the use of flights promotes homogeneity and uniformity, the wide size distribution of lateritic ore (Table 1) and small peaks of tracer concentration also suggested particle segregation [19]. Segregation is an intensive property of dry granular solids, which tend to separate spatially by shape, size, or density under varying conditions of the flow [62]. Furthermore, ore moisture causes adhesion of the material to the flights and walls, causing retention of the tracer within the dryer [18]. Consequently, the quality of adjustment of solid transport models may be affected.

Furthermore, some parameters proposed fluid non-ideal and intermediate between plug flow and complete mixing, such as $k_3$, $k_4$ and $k_5$ (Table 8).

[29] was the most representative of the tracer distribution within the dryer, with a determination coefficient ($R^2$) ranged between 92.32 % and 94.77 %, the lower (*ARE*) and (*MPSD*). For dryer D-1, both the main and side branches were characterized to provide a high mixing level, $n = 35$ and $m = 50$, respectively, non-ideal flow fraction (*f*) was 15 % of total fluid, the residence time estimated $\alpha^{-1} = 71.9$ % of the experimental time ($t_m$). This behavior is consistent with a hydraulic efficiency of 123 % (Table 9).

From Table 9, the highest deviation between estimations and measurements were for Tanks-in-series model, followed by Martin et al. (2005) and Open Axial Dispersion. This is interpreted as because of some assumptions of the predicted model do not apply for the lateritic ore distribution. These models were not in good agreement with measurements since present lower $R^2 < 85.2$ %, and relatively higher ARE and MPSD values.

### 3.2. Performance indicators of mass and heat transfer

Following the "black box" model from Fig. 4, the mass and heat balances were carried out in the drying system at an ore input flow rate of 40 t $h^{-1}$, 45 t $h^{-1}$ and 50 t $h^{-1}$ (dry basis).

The unknown variables were fuel flow; drying gas flow, which consist of two partial flows, flue gas and secondary air (see Fig. 3), its chemical composition, temperature and specific heat; as well as the final moisture of drying gas. These variables were determined through an iterative process, and then, the results were verified through the law of conservation of mass, for a relative error (ξ) of 0.01 % (Table 10).

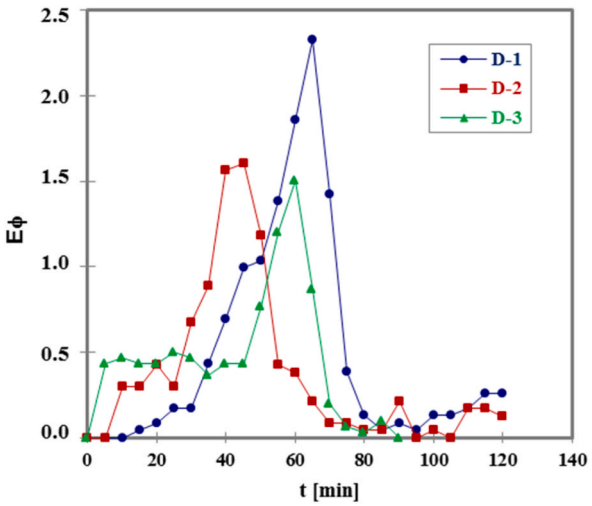


**Fig. 5.** Normalized Residence time distribution (RTD) of the ore transport through flighted rotary dryers at a productivity of 45 t $h^{-1}$ (dry ore).

**Table 7**
Theoretical residence time in the flighted rotary dryer for $G_s$: 15.8 kg $s^{-1}$ and $L_s$: 12.5 kg $s^{-1}$

| Models: | Friedman and Marshall (1949) | Putton (1942) | Saeman and Mitchell (1954) | Kelly (1995) | Karali et al. (2020) | $\bar{t}_0$ |
|---|---|---|---|---|---|---|
| $t_0$ [min] | 48 | 53 | 49 | 53 | 52 | 51 ± 2 |

**Table 8**
Parameters of (RTD) in the flighted rotary dryer at Ls 45 t $h^{-1}$

| Dryer (D) | 1 | 2 | 3 | |
|---|---|---|---|---|
| $t_m$ [min] | 61 | 46 | 44 | Experimental mean residence time |
| $k_0 = \frac{t_m}{t_0}$ | 1.23 | 0.92 | 0.88 | Hydraulic efficiency $t_0 = 50$ min |
| Σ | 63.88 | 49.52 | 46.76 | Second moment RTD, Eq. (38) |
| $k_1 = \frac{t_a}{t_0}$ | 0.49 | 0.22 | 0.23 | $t_a$: Time recorded when the selected tracer presents in the outlet; $t_0$: The theoretical time. $k_1 = 0$ for Mixed flow; $k_1 < 0.3$ for Hydraulic short – circuit; $k_1 = 1$ for Plug flow |
| $k_2 = \frac{t_{50}}{t_0}$ | 1.01 | 0.92 | 1.09 | $t_{50}$: Time required for 50 % of the selected tracer leaves. $k_2 < 1$ for hydraulic short – circuits; $k_2 > 1$ for experimental errors or stagnant zones. |
| $k_3 = \frac{t_p}{t_0}$ | 1.06 | 0.98 | 1.38 | $t_p$: Time required for the presentation of the maximum tracer amount. $k_3 \sim 0$ for Mixed Model; $k_3 \sim 1$ and $k_1 > 0.5$ for Plug flow |
| $k_4 = \frac{t_c}{t_0}$ | 0.90 | 0.76 | 1.15 | $t_c$: Time required for the concentration to be 50 % of the maximum tracer amount. $k_4 \geq 0.693$ for Complete mix |
| $k_5 = \frac{t_b}{t_0}$ | 0.57 | 0.22 | 0.11 | $t_b$: Time recorded when the concentration is 1/10 of the maximum tracer amount. $k_5 \sim 2.3$ for Complete mix |

**Table 9**
Modelling parameters of the (RTD) function in the flighted rotary dryer at Ls 45 t $h^{-1}$ (dry basis).

| Rotary dyer (D) | 1 | 2 | 3 | Descriptions |
|---|---|---|---|---|
| | Tanks-in-series model | | | |
| *N* | 33 | 15 | 12 | Equal-sized CSTR |
| $R^2$ [%] | 85.65 | 85.70 | 9.07 | Determination coefficients |
| *ARE* | 2.56 | 2.03 | 2.36 | Average Relative Error |
| *MPSD* | 1.35 | 0.82 | 1.21 | Marquardt's Percent Standard Deviation |
| | Open Axial Dispersion Model | | | |
| $\sigma^2$ | 375 | 497 | 399 | Distribution width |
| $\sigma_\theta^2$ | 0.10 | 0.23 | 0.21 | Normalized variance |
| *Bo* | 0.015 | 0.033 | 0.033 | Peclet–Bodenstein module |
| $R^2$ [%] | 82.67 | 77.94 | 9.35 | Determination coefficients |
| ARE | 1.15 | 0.92 | 0.99 | Average Relative Error |
| MPSD | 1.83 | 1.15 | 1.26 | Marquardt's Percent Standard Deviation |
| | Himmelblau and Bischoff's model (1968) | | | |
| *A* | 1.39 | 0.95 | 1.85 | Ratio between the main and the side branch |
| *F* | 0.15 | 0.60 | 0.53 | Total fluid flow to side branch (fraction) |
| *M* | 50 | 50 | 90 | Number of tanks in the main branch flow |
| *N* | 35 | 4 | 2 | Number of tanks in the side branch flow |
| $R^2$ [%] | 90.32 | 94.77 | 92.47 | Determination coefficients |
| *ARE* | 0.87 | 0.59 | 0.22 | Average Relative Error |
| *MPSD* | 1.12 | 0.86 | 0.09 | Marquardt's Percent Standard Deviation |
| | Martin, et al. model (2005) | | | |
| *N* | 40 | 25 | 12 | Equal-sized CSTR continuous flow |
| *1-n* | 0.10 | 0.20 | 0.015 | Bypassing (fraction) |
| *1-M* | 0.01 | 0.02 | 0.01 | Dead-spaces (fraction) |
| *δ* | 0.011 | 0.011 | 0.033 | Dirac delta function |
| $R^2$ [%] | 85.16 | 85.12 | 0.57 | Determination coefficients |
| *ARE* | 0.91 | 0.69 | 1.00 | Average Relative Error |
| *MPSD* | 1.41 | 0.91 | 1.32 | Marquardt's Percent Standard Deviation |

The sources of consumption and heat losses are shown in Table 11. The inlet drying gas temperature ($T_G$ int) resulted between 860 °C and 871 °C. A potential reduction in fuel consumption can be obtained by increasing the temperature of secondary air ($Q_6$), also using hot gases from other stages of the industrial process.

From the above results, performance indicators were determined for the rotary dryer of nickel laterite ore (Table 12).

Specific fuel consumption ($r_1$) was an average 27.25 ± 0.25 kg fuel per ton of wet ore, and specific energy consumption ($r_2$) 79.66 ± 0.95 kg fuel per ton of $H_2O$ evaporated, these values exceeded the target indexes in the industry ($r_1$: 25.65 kg $t^{-1}$, $r_2$: 72.96 kg $t^{-1}$). In this work, the $H_2O$ evaporated coming from ore moisture, fuel, primary and secondary air.

**Table 10**
Mass balance in the flighted rotary dryer by "black box" model.

| Current | Variable | Code | Unit | Dry ore flow, Ls [kg $h^{-1}$] (Current 5) | | |
|---|---|---|---|---|---|---|
| | | | | 40000 | 45000 | 50000 |
| 1 | Wet ore | $L_1$ | kg $h^{-1}$ | 59701.50 | 67164.18 | 74626.87 |
| 2 | Fuel flow | $w_2$ | kg $h^{-1}$ | 1611.94 | 1830.22 | 2052.24 |
| 3 | Wet primary air | $w_3$ | kg $h^{-1}$ | 27063.40 | 30728.24 | 34455.72 |
| 4 | Wet secondary air | $w_4$ | kg $h^{-1}$ | 20855.55 | 24195.21 | 27479.00 |
| 6 | Combustion gas | $w_4$ | kg $h^{-1}$ | 28665.84 | 32547.67 | 36495.86 |
| 7 | $H_2O$ vapor from ore | $w_6$ | kg $h^{-1}$ | 18034.83 | 20289.18 | 22543.53 |
| 8 | Dry residue | $w_4$ | kg $h^{-1}$ | 0.81 | 0.92 | 1.03 |
| Total inlet (currents 1 to 4) | | $W_{int}$ | kg $h^{-1}$ | kg $h^{-1}$ | 123917.85 | 138613.82 |
| Total outlet (currents 5 to 8) | | $W_{out}$ | kg $h^{-1}$ | kg $h^{-1}$ | 123908.02 | 138602.79 |
| Relative error | | $\xi$ | % | 0.01 | 0.01 | 0.01 |

**Table 11**
Energy balance in the flighted rotary dryer by "black box" model.

| Dry ore flow, Ls [kg $h^{-1}$] | | 40000 | | 45000 | | 50000 | |
|---|---|---|---|---|---|---|---|
| Variable | Code | Energy | | | | | |
| | | kW | % | kW | % | kW | % |
| Ore heating and evaporation of ore moisture | $Q_1$ | 12593.2 | 68.11 | 14167.3 | 67.53 | 15741.5 | 66.84 |
| $H_2O$ evaporation contained in the fuel | $Q_2$ | 534 | 2.89 | 601 | 2,87 | 668 | 2,84 |
| $H_2O$ formation by hydrogen combustion of fuel | $Q_3$ | 3.9 | 0.02 | 4.4 | 0,02 | 4.9 | 0,02 |
| $H_2O$ evaporation contained in primary air | $Q_4$ | 10.3 | 0.06 | 11.7 | 0.06 | 13.1 | 0.06 |
| Air secondary heating | $Q_5$ | 5.3 | 0.03 | 6.0 | 0.03 | 6.7 | 0.03 |
| $H_2O$ evaporation contained in secondary air | $Q_6$ | 4961.6 | 26.84 | 5754.7 | 27.43 | 6627.0 | 28.14 |
| Dry gassy products | $Q_7$ | 4.05 | 0.02 | 4.70 | 0,02 | 5.33 | 0,02 |
| Incomplete combustion | $Q_8$ | 347.8 | 1.88 | 398.3 | 1,90 | 449.1 | 1,91 |
| Non burnt carbon | $Q_9$ | 0.0 | 0.00 | 0.0 | 0,00 | 0.0 | 0,00 |
| Radiation, convection and conduction | $Q_{10}$ | 0.0 | 0.00 | 0.0 | 0,00 | 0.0 | 0,00 |
| Energy entered into the system, by Eq. (20) | $Q_0$ | 27.9 | 0.15 | 31.7 | 0.15 | 35.6 | 0.15 |
| Total useful energy ($Q_1$-$Q_6$), by Eq. 21–28 | $Q_{11}$ | 18112.60 | | 20549.90 | | 26066.50 | |
| Total energy losses ($Q_7$-$Q_{10}$), by Eq. 29–34 | $Q_{12}$ | 375.80 | | 430.00 | | 484.68 | |
| Relative error | $\xi$ | | 0.72 | | 0.77 | | 0.66 |

**Table 12**
Performance indicators in the flighted rotary dryer for lateritic ore drying.

| Indicator | Dry ore flow, Ls [kg $h^{-1}$] | | |
|---|---|---|---|
| | 40000 | 45000 | 50000 |
| Specific fuel consumption [kg fuel $t^{-1}$ of wet ore] | 27.00 | 27.25 | 27.50 |
| Specific energy consumption [kg fuel $t^{-1}$ of $H_2O$ evaporated] | 78.83 | 79.45 | 80.07 |
| Energy efficiency [%] | 97.27 | 97.29 | 97.29 |
| Thermal efficiency [%] | 67.70 | 66.47 | 66.47 |
| Drying efficiency [%] | 98.64 | 98.78 | 98.88 |

Furthermore, the energy efficiency, assumed as the ratio of the total energy consumed to the maximum theoretical energy that can be supposed from the system [2] ($Q_{11}/Q_0$), was 97.28 ± 0.01 %; the thermal efficiency, which consist of amount of energy performed to evaporate 1 kg of water (96.3 % $Q_1$+ $Q_2$+ $Q_4$ + $Q_6$) • $Q_0^{-1}$ of 66.88 ± 0.71 %; and drying efficacy, evaluated considering the initial, final, and equilibrium moisture contents [28] of 98.77 ± 0.12 %.

The simulation of drying process was made based on the mathematical model depicted in Section 2.3.3, considering the results of the "black box" model referring to flows, composition and temperature. The temperature profile along the rotary dryer of the two streams into gas and solid phase are shown in Fig. 6 a, b.

The simulation predicted an increase of ore temperatures at a decreasing rate up to 206 °C, which can be appreciated with an ore temperature peak near the drum inlet, approximately at the firth 1.5 m long. After that, the temperature remained fairly constant and finally decreased with value close to the gas temperature. This is typical behavior concurrent rotary dryer [2]. Simultaneously, the inlet ore moisture (X) decreased exponentially from 0.4925 kg $H_2O$ $kg^{-1}$ to 0.033 kg $kg^{-1}$ dry basis (Fig. 6c), due to moisture (X) in every instant depends on the evolutions of the moisture gradient within the ore (internal driving force), Eq. (60), and drying gas temperature ($T_G$) by the Arrhenius equation, Eq. (61).

In that order of ideas, according to Fig. 6d, with raise in temperature of drying medium ($T_G$) the amount of heat provided to the ore tends to increase and therefore the drying rate increases [17]; in turn, increase of drying medium moisture (Y) (Fig. 6c) and $T_G$

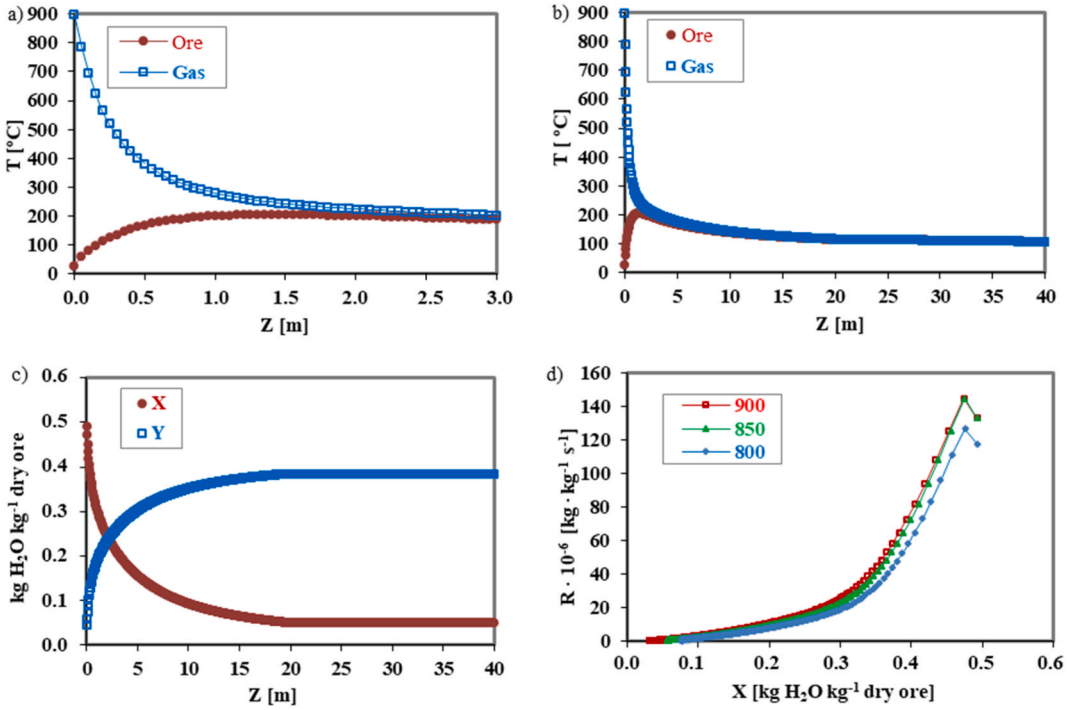


**Fig. 6.** Drying of lateritic ore at Ls 45 t $h^{-1}$ and 28.5 kg fuel $t^{-1}$ wet ore; a, b) Temperature profiles along the rotary dyer, c) Moisture profile, gaseous phase (Y) and solid phase (X), d) Drying Rate at different inlet gas temperature ($T_G$, °C).

decreases (Fig. 6a) by Eq. (56). This is interpreted as moisture difference between the bulk gas and the local moisture content of the ore surface act as driving force external [5,63].

Although the rate of drying depends on the drying gas, the product, and the geometrical configuration of the dryer, the above results suggest that the Arrhenius equation is suitable for modelling the drying rate of lateritic ore, resulting final moisture between 4.17 and 5.2 % (dry basis) according to target moisture.

As the inlet ore moisture or dryer productivity increases, the amount of water to be evaporated increases too; thus it is essential to enhance the heat transfer rate from gas to product [21,22]. According to mathematical modelling results, an increase in the temperature of the inlet drying gas ($T_G$ int) (flue gas and secondary air) reduces exponentially the ore moisture content in the outlet stream at dryer productivity between 40 t $h^{-1}$ and 50 t $h^{-1}$ (dry basis) and initial moisture 0.33 kg $H_2O$ $kg^{-1}$ wet solid (Fig. 7).

Fig. 7 also indicate that the best temperature was 900 °C resulting in moisture between 3.0 % and 4.54 %; while at 850 °C the moisture varied from 3.81 % to 7.12 %. Inlet gas temperature ($T_G$) predictions presented a good agreement between the mathematical model, "black box" model ($860 \leq T_G \leq 871$ °C), and the target temperature ($T_G = 900$ °C maximum). In addition, Fig. 7 suggest that solid feed rate is a solution to attaining target ore moisture in comparison to performing the gas influent temperature to control the product moisture content, due to this increases the consumption of fuel throughout the combustion chamber [18].

The outlet moisture content presented an exponential relationship with inlet moisture ($0.22 \leq x \leq 0.36$ kg $H_2O$ $kg^{-1}$ wet ore) under constant operation conditions (Fig. 8). Therefore, any change in this variable affects the outlet moisture and, consequently, the productivity and the specific consumption of energy in the dryer's operating zone [21,23]. This highlights the benefits of minimizing the solid's inlet moisture content, as much as possible, by solar drying [64–66].

The final gas temperature ($T_G$ out) remained approximately constant with a variation of dryer productivity from 40 t $h^{-1}$ to 50 t $h^{-1}$; but the final moisture (x out) ranged from 0.024 to 0.126 kg $H_2O$ $kg^{-1}$ wet ore at an inlet temperature ($T_G$ int) of 900 °C. This is interpreted as the productivity threshold to the maximum mass and heat transfer. The relationship between both variables followed a double inverse function, with a coefficient of determination adjusted by the degrees of freedom of 95 % (Fig. 9).

From Fig. 9, for final ore moisture between 0.030 and 0.052 kg $H_2O$ $kg^{-1}$ wet ore, the final temperature of drying gas ($T_G$) (equal to final ore temperature) resulted from 92 °C to 100 °C, which is coherent with target temperature threshold of 75–110 °C and the set up value to mass and energy balance of 90 °C.

The heat loss determined by mass and energy balance presented a mean relative error of $2.10 \pm 1.22$ % with regard to mean heat in control volumes of dryer (dz) by Aruda's model, Eq. (57).

The most suitable manipulated variable for different operational conditions was identified by the approach of Duchesne et al. (1997). Ore moisture content (x int) and drying gas temperature ($T_G$ int) were considered as input variables (manipulated). On the other hand, the output variables (controlled) were: ore moisture content (x out) and gas temperature ($T_G$ out) (Table 13 and Table 14).

The relative indices showed that inlet $T_G$ has the higher significant on product moisture content in an opposite relationship, which

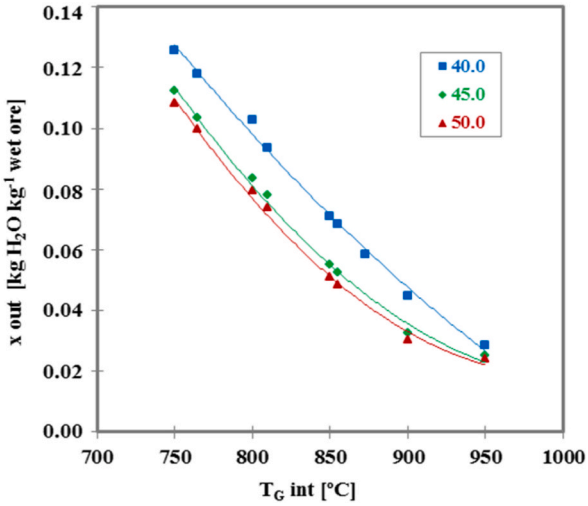


**Fig. 7.** Effect of inlet dryer gas temperature variations on the outlet ore moisture, at inlet ore moisture 0.33 kg $H_2O$ $kg^{-1}$ solid and different ore rate (Ls, t $h^{-1}$) (wet basis).

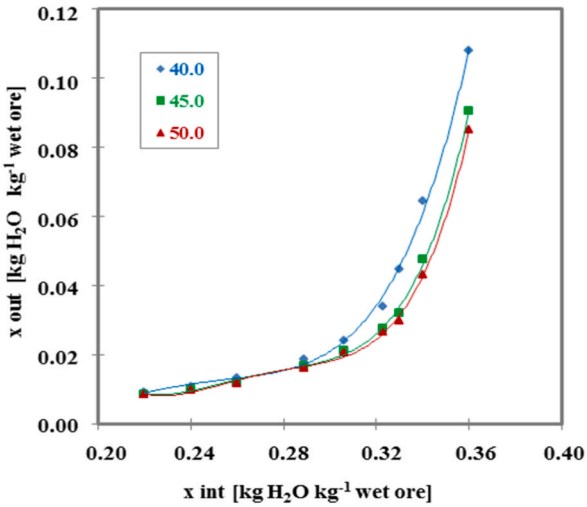


**Fig. 8.** Effect of inlet ore moisture variations on outlet moisture at inlet $T_G$ 900 °C and different ore rate (Ls, t $h^{-1}$) (wet basis).

is consistent with Fig. 9. It should note that at a scaled to 3 %, both input variables enhance drying rate with similar extent.

Although inlet ore moisture has reduced effect on decreasing the product moisture at a scaled to 15 % in a direct relationship (see Table 14 and Fig. 9), its effect is much more significant on lowering both final temperature gas and product in an opposite relationship.

Based on previous results, it is suggested to develop a computerized system for the modelling and simulation of lateritic ore drying that implements these algorithms, with features that facilitate evaluating the operating parameters and deciding a better operation and control strategy. It is necessary to carry out a detailed characterization of the dryers as for the geometric design parameters of flighted rotary dryer, taking into account results of the bibliographic review. Combining the hydrodynamic and mathematical models can results in ore moisture prediction with much more successful outcomes. Furthermore, future research should be done in order to enhance drying kinetics model and the heat transfer coefficient in this system.

## 4. Conclusions

Some performance indicators related to momentum, mass and heat transfer were evaluated in the drying process of Cuban nickel laterite ore within flighted rotary dryer. As a result: The solid transport was approached to the model of multi-branch tanks-in-series with the highly significant goodness of fit ($R^2$) ranged between 90.32 % and 94.77 %. For a hydraulic efficiency ($t_m/t_0$) higher than 1, the solid transport was categorized to present a high mixing level in the branches, the fraction of non-ideal flow was 15 % of total fluid due to dead-spaces and so, experimental mean residence time ($t_{m-1} = 60$ min) was higher than the theoretical residence time ($t_0 = 51$

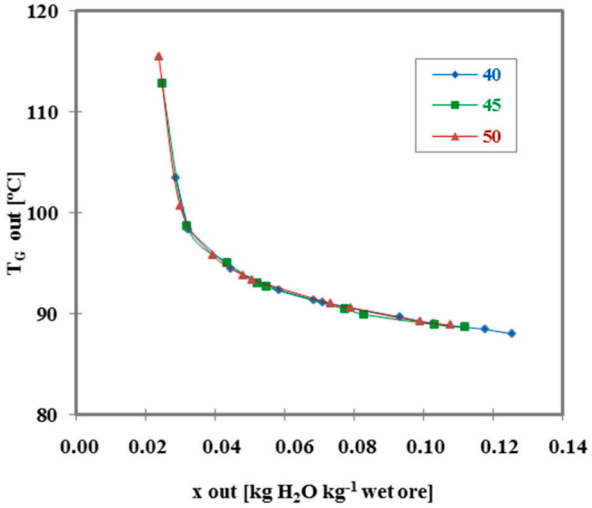


**Fig. 9.** Interaction between outlet gas temperature and outlet ore moisture at the inlet conditions: ore moisture 0.33 kg $H_2O$ $kg^{-1}$ solid, $T_G$ 900 °C and different ore rate (Ls, t $h^{-1}$) (wet basis).

**Table 13**
Relative index of output variables for change in the inlet gas temperature at 0.33 kg $H_2O$ $kg^{-1}$ wet solid.

| Scaled [%] | $T_G$ int [°C] | 40 t $h^{-1}$ | | 45 t $h^{-1}$ | | 50 t $h^{-1}$ | |
|---|---|---|---|---|---|---|---|
| | | x out | $T_G$ out | x out | $T_G$ out | x out | $T_G$ out |
| | 900 | | | | | | |
| −3 | 873 | −10.29 | 0.74 | −12.13 | 1.22 | −10.51 | 1.61 |
| −5 | 855 | −10.59 | 0.64 | −12.59 | 1.13 | −12.11 | 1.36 |
| −10 | 810 | −10.87 | 0.50 | −14.15 | 0.83 | −14.47 | 0.96 |
| −15 | 765 | −10.87 | 0.42 | −14.79 | 0.66 | −15.39 | 0.76 |

**Table 14**
Relative index of output variables for change in the inlet ore moisture at $T_G$ 900 °C.

| Scaled [% | x int [g $kg^{-1}$] | 40 t $h^{-1}$ | | 45 t $h^{-1}$ | | 50 t $h^{-1}$ | |
|---|---|---|---|---|---|---|---|
| | | x out | $T_G$ out | x out | $T_G$ out | x out | $T_G$ out |
| | 0.340 | | | | | | |
| −3 | 0.330 | 10.34 | −0.87 | 11.11 | −1.63 | 10.42 | −2.05 |
| −5 | 0.323 | 9.47 | −1.17 | 8.34 | −2.33 | 7.65 | −2.67 |
| −10 | 0.306 | 6.24 | −2.31 | 5.53 | −3.01 | 5.25 | −3.18 |
| −15 | 0.289 | 4.71 | −2.82 | 4.31 | −3.28 | 4.15 | −3.38 |

± 2 min). For a hydraulic efficiency ($t_m/t_0$) less than 1, the solid transport showed a high mixing level in the main branch flow, and low level of mixing in the side branch. The non-ideal flow fraction was 53 % and 60 % due to short-circuit, resulting in a smaller experimental mean residence time, 44 min and 46 min, respectively. At productivity between 40 t $h^{-1}$ and 50 t $h^{-1}$ (dry basis), the specific fuel consumption was 27.25 ± 0.25 kg fuel per ton of wet ore; specific energy consumption 79.66 ± 0.95 kg fuel per ton of $H_2O$ removed; energy efficiency 97.28 ± 0.01 %; and the thermal efficiency 66.88 ± 0.71 %. The ore feed rate between 45 t $h^{-1}$ and 50 t $h^{-1}$ propitiates the better heat and mass transfer to achieving target ore moisture. The temperature of the inlet drying gas between 873 °C and 900 °C results in outlet ore moisture between 3.00 % and 4.38 %, under the above condition, the inlet ore moisture must be less than 34 % (wet basis). Input variables drying gas temperature and ore moisture, exhibits the higher significant on the output variables product moisture and outlet gas temperature respectively, in an opposite relationship. Thus, both input variables could be used in conjunction to better control the rotary dryer. The algorithms proposed for "black box" model and mathematical modelling can be used to decide the better operation strategy and control of ore drying. In addition, future research should be conducted to achieve major adequacy of both drying kinetics model and heat transfer coefficient to this industrial system.

## Data availability statement

The data used to support the findings of this study are included within the article.

## Additional information

No additional information is available for this paper.

## CRediT authorship contribution statement

**Armando Rojas Vargas:** Writing – review & editing, Visualization, Investigation, Formal analysis, Data curation. **Liudmila Pérez García:** Writing – review & editing, Writing – original draft, Visualization, Validation, Resources, Methodology, Investigation, Data curation, Conceptualization. **Crispin Sánchez Guillen:** Writing – review & editing, Writing – original draft, Visualization, Validation, Supervision, Software, Project administration, Data curation, Conceptualization. **Forat Yasir AlJaberi:** Writing – review & editing, Writing – original draft, Methodology, Formal analysis, Data curation. **Ali Dawood Salman:** Writing – review & editing, Writing – original draft, Visualization, Validation, Software, Methodology, Investigation, Formal analysis, Data curation. **Saja Mohsen Alardhi:** Writing – review & editing, Writing – original draft, Visualization, Validation, Resources, Investigation, Formal analysis, Data curation. **Phuoc-Cuong Le:** Writing – review & editing, Writing – original draft, Supervision, Software, Project administration, Methodology, Funding acquisition.

## Declaration of competing interest

The authors declare that they have no known competing financial interests or personal relationships that could have appeared to influence the work reported in this paper.

## Acknowledgments

The authors are grateful to corporative group for the production of nickel in Cuba, as well as they are grateful to the Ministry of Education and Training of Vietnam with project (B2022-DNA-04), for their generous support of this research.

## Nomenclature

*List of symbols*

| | |
|---|---|
| $T_R$ | Reference temperature [°C] |
| $C$p | Specific heat [kJ (kg °C)$^{-1}$] |
| $D$ | Drum diameter [m] |
| $D$p | Particle mean diameter [mm] |
| $f_v$ | Fraction of drum cross section occupied by solids [−] |
| $G_s$ | Dry gas flow [kg•h$^{-1}$] |
| $G'_s$ | Dry gas flow [kg m$^{-2}$ s$^{-1}$] |
| $H$ | Enthalpies [kJ kg$^{-1}$] |
| $L$ | Drum length [m] |
| $l$ | Two segment flights length [m] |
| $L_s$ | Dry solid flow [t h$^{-1}$] |
| $L'_s$ | Dry solid flow [kg m$^{-2}$ s$^{-1}$] |
| $n$ | Number of rotations per minute [rpm] |
| $N$m | Number of mineral [−] |
| $Q_p$ | Lost heat [kJ kg$^{-1}$] |
| $r$ | Inside radius [m] |
| $r_H$ | Effective radial distance [m] |
| $r_0$ | Outside radius [m] |
| $t_0$ | Time [min] |
| $T_G$ | Dryer gas temperature (flue gas and secondary air) [°C] |
| $U$ | Volumetric heat transfer coefficient [kW m$^{-3}$ K$^{-1}$] |
| $U_p$ | Heat loss coefficient [kW m$^{-3}$ K$^{-1}$] |
| $x_s$ | Solid moisture [kg $H_2O$ kg$^{-1}$] dry solid |
| $Y_s$ | Gas moisture [kg $H_2O$ kg$^{-1}$] dry solid |

*Greek symbols*

| | |
|---|---|
| $\alpha_1$ | Angulations in flights [rad] |
| $\gamma$ | kinetic angle of repose [rad] |
| $\delta$ | flight's discharge angle [rad] |
| $\Theta$ | Dynamic angle of repose [rad] |
| $\lambda$ | Cylinder tild angle [rad] |
| $\tau_0$ | Experimental |

*Indices*

| | |
|---|---|
| ai | Air |
| aip | Primary air |
| Int | Inlet |
| Out | Outlet |
| s | Dry |
| w | Water |

## References


[1] P. Zdzisław, Algorithmic approach to process design of direct rotary dryers-coolers, Dry. Technol. (2020), https://doi.org/10.1080/07373937.2020.1841789.
[2] A. Echeeri, M. Maalmi, Performance evaluation of a rotary dryer in both co-current and counter-current configurations, J. Therm. Eng. 7 (14) (2021) 1945–1957, https://doi.org/10.18186/thermal.1051277.
[3] J. Seidenbecher, F. Herz, K.R. Sunkara, J. Mellmann, Modelling the final discharge angle in flighted rotary drums, Granul. Matter 24 (123) (2022), https://doi.org/10.1007/s10035-022-01283-x.
[4] H. Perazzini, F.F. Bentes, J.F. Teixeira, Prediction of residence time distribution of solid wastes in a rotary dryer, Dry. Technol.: Int. J. 32 (4) (2014) 428–436, https://doi.org/10.1080/07373937.2013.835317.
[5] M.I.H. Khan, C.P. Batuwatta-Gamage, M.A. Karim, Y. Gu, Fundamental understanding of heat and mass transfer processes for physics-informed machine learning-based drying modelling, Energies 15 (9347) (2022), https://doi.org/10.3390/en15249347.
[6] O.O. Ajayi, M.E. Sheehan, Design loading of free flowing and cohesive solids in flighted rotary dryers, Chem. Eng. Sci. 73 (2012) 400–411, https://doi.org/10.1016/j.ces.2012.01.033.
[7] A.J. Matchett, G.J. Baker, Particle residence time in cascading rotary dryer, Part. I. Derivación of the two-stream model, J. Sep. process Technol. 8 (1987) 11–17.
[8] D. Revol, C.L. Briens, J.M. Chabagno, The design of flights in rotary dryers, Powder Technol. 121 (2–3) (2001) 230–238, https://doi.org/10.1016/S0032-5910(01)00362-X.
[9] N.J. Fernandes, C.H. Ataíde, M.A.S. Barrozo, Modeling and experimental study of hydrodynamic and drying characteristics of an industrial rotary dryer, Braz. J. Chem. Eng. 26 (2) (2009) 331–341. https://www.scielo.br/j/bjce/a/sRmbXjnPYwMTx9gNkrnKQWS/?lang=en.
[10] M.A. Karali, K.R. Sunkara, F. Herz, E. Specht, Experimental analysis of a flighted rotary drum to assess the optimum loading, Chem. Eng. Sci. 138 (2015) 772–779, https://doi.org/10.1016/j.ces.2015.09.004.
[11] K.R. Sunkara, F. Herz, E. Specht, J. Mellmann, Influence of flight design on the particle distribution of a flighted rotating drum, Chem. Eng. Sci. 90 (2013) 101–109, https://doi.org/10.1016/j.ces.2012.12.035.
[12] J.C. Silveira, R.J. Brandao, R.M. Lima, M.V.C. Machado, M.A.S. Barrozo, C.R. Duarte, A fluid dynamic study of the active phase behavior in a rotary drum with flights of two and three segments, Powder Technol. 368 (2020) 297–307, https://doi.org/10.1016/j.powtec.2020.04.051.
[13] R.A. Vargas, S.C. Guillén, M.E.M. Haynes, F.Y. AlJaberi, Nickel removal from an industrial effluent by electrocoagulation in semi-continuous operation: hydrodynamic, kinetic and cost analysis, Results Eng. 17 (2023), 100961, https://doi.org/10.1016/j.rineng.2023.100961.
[14] M. Krokida, D. Marinos-Kouris, A.S. Mujumdar, Rotary drying. Ch. 7, in: A.S. Mujumdar (Ed.), Handbook of Industrial Drying, third ed., CRC Press, Boca Raton, 2006, pp. 151–172.
[15] S.J. Friedman, W.R. Marshall, Studies in rotary drying, Part I, Chem. Eng. Prog. 45 (8) (1949) 482–493.
[16] C. Duchesne, J. Thibault, C. Bazin, Modeling of the solids transportation within an industrial rotary dryer: a simple model, Ind. Eng. Chem. Res. 35 (7) (1996) 2334–2341, https://doi.org/10.1021/ie950625j.
[17] P.S.T. Sai, Drying of solids in a rotary dryer, Dry. Technol.: Int. J. 31 (2) (2013) 213–223, https://doi.org/10.1080/07373937.2012.711406.
[18] O.O. Ajayi, Multiscale Modelling of Industrial Flighted Rotary Dryers, PhD Thesis, James Cook University, 2011, http://eprints.jcu.edu.au/28051/.
[19] A.S.B. Njeng, Experimental study and modeling of hydrodynamic and heating characteristics of flighted rotary kilns. These en vue de l'obtention du doctorat. Ecole des Mines d'Albi-Carmaux. Francia, 2015, p. 310. https://theses.hal.science/tel-01291791/.
[20] F. Castaño, R.F. Rubio, M.G. Ortega, Modelado de Secaderos Rotatorios en Isocorriente, RIAI 6 (4) (2009) 32–43, https://doi.org/10.1016/S1697-7912(09)70106-2.
[21] H. Abbasfard, H.H. Rafsanjani, S. Ghader, M. Ghanbari, Mathematical modeling and simulation of an industrial rotary dryer: a case study of ammonium nitrate plant, Powder Technol. 239 (2013) 499–505, https://doi.org/10.1016/j.powtec.2013.02.037.
[22] D. Friso, Mathematical modelling of rotary drum dryers for alfalfa drying process control, Inventions 8 (2023) 11, https://doi.org/10.3390/inventions8010011.
[23] K. Ettahi, M. Chaanaoui, V. Sébastien, S. Abderafi, T. Bounahmidi, Modeling and design of a solar rotary dryer bench test for phosphate sludge, Model. Simulat. Eng. (2022) 1–11, https://doi.org/10.1155/2022/5574242.
[24] C. Zalazar-Oliva, E. Góngora-Leyva, A.A. Legrá-Lobaina, M.A. León-Segovia, M.-A. León-Segovia, H.L. Laurencio-Alfonso, Modelación matemática del secado de menas lateríticas de Ni en un horno cilíndrico rotatorio a escala semindustrial, Miner. Geol. 38 (4) (2023) 346–362. http://revista.ismm.edu.cu/index.php/revistamg/article/view/2240.
[25] C.A. Pickles, Drying kinetics of nickeliferous limonitic laterite ores, Miner. Eng. 16 (12) (2003) 1327–1338, https://doi.org/10.1016/s0892-6875(03)00206-1.
[26] M. Kaveh, Y. Abbaspour-Gilandeh, G. Chen, Drying kinetic, quality, energy and exergy performance of hot air-rotary drum drying of green peas using adaptive neuro-fuzzy inference system, Food Bioprod. Process. 124 (2020) 168–183, https://doi.org/10.1016/j.fbp.2020.08.011.
[27] K. Nwosu-Obieogu, O.E. Olusola, S. Bright, Energy and exergy analysis of three leaved yam starch drying in a tray dryer: parametric, modelling and optimization studies, Heliyon 8 (2022), e10124, https://doi.org/10.1016/j.heliyon.2022.e10124.
[28] F.J.G. La Cruz, A. Palomar-Torres, J.M.P. Carnicero, F. Cruz-Peragón, Energy and exergy analysis during drying in rotary dryers from finite control volumes: applications to the drying of olive stone, Appl. Therm. Eng. 200 (2022), 117699, https://doi.org/10.1016/j.applthermaleng.2021.117699.
[29] D.M. Himmelblau, K.B. Bischoff, Process Analysis and Simulation: Deterministic Systems, John Wiley & Sons, Inc., New York, NY, 1968.
[30] M. Ayers, Residence time distribution of mixing based on mathematical modeling, Honors Res. Proj. 604 (2018). http://ideaexchange.uakron.edu/honors_research_projects/604.
[31] A. Sonsiri, V. Punyakum, T. Radpukdee, Optimal variables estimation for energy reduction via a remote supervisory control: application to a counter-flow rotary dryer, Heliyon 5 (1) (2019), e01087, https://doi.org/10.1016/j.heliyon.2018.e01087.
[32] T.E. Torres, M.R. Galano, G.E. Efraím, Análisis de la influencia del régimen de temperatura en el secado del mineral laterítico, Miner. Geol. 1–2 (2003) 119–123. http://revista.ismm.edu.cu/index.php/revistamg/article/view/239.
[33] R.H. Perry, D.W. Green, Perry's Chemical Engineering's Handbook, seventh ed., McGraw-Hill, New York, 1999. ISBN 0-07-049841-5.
[34] E.B. Arruda, Comparison of the Performance of the Roto-Fluidized Dryer and Conventional Rotary Dryer, Ph.D. thesis, Federal University of Uberlandia, Uberlandia, Brazil, 2006.
[35] A.R. Vargas, M.E.T. Nieves, Y.G. Díaz, Ammoniacal Carbonate Leaching: effect of dissolved sulfur in the distillation operation, Acta Chim. Slov. 67 (2020) 1239–1249, https://doi.org/10.17344/acsi.2020.6147.

[36] O. Krauze, D. Buchczik, S. Budzan, Measurement-based modelling of material moisture and particle classification for control of copper ore dry grinding process, Sensors 21 (2) (2021) 667, https://doi.org/10.3390/s21020667.
[37] D. Saramak, R.A. Kleiv, The effect of feed moisture on the comminution efficiency of HPGR circuits, Miner. Eng. 43–44 (2013) 105–111, https://doi.org/10.1016/j.mineng.2012.09.014.
[38] A.R. Vargas, C.G. Sánchez, M.E.H. Magaña, C.P. Hernández, Extracción potential de níquel y cobalto con mineral laterítico de mina "Pinares de Mayarí" en la tecnología Caron. Parte I, Tecnol. Quím. 41 (3) (2021) 523–535. https://tecnologiaquimica.uo.edu.cu/index.php/tq/article/view/5208.
[39] M.G.G. Mazza, L.E.B. Brandão, G.S. Wildhagen, Characterization of the residence time distribution in spray dryers, Dry. Technol.: Int. J. 21 (3) (2003) 525–538, https://doi.org/10.1081/DRT-120018460.
[40] P. Toson, P. Doshi, D. Jajcevic, Explicit residence time distribution of a generalised cascade of continuous stirred tank reactors for a description of short recirculation time (bypassing), Processes 7 (2019) 615, https://doi.org/10.3390/pr7090615.
[41] Y. Gao, F.J. Muzzio, M.G. Ierapetritou, A review of the Residence Time Distribution (RTD) applications in solid unit operations, Powder Technol. 228 (2012) 416–423, https://doi.org/10.1016/j.powtec.2012.05.060.
[42] S. Meenakshi, C. Avinash, B. Haripada, K.B. Pramod, J.P. Harish, Residence time distribution studies using radiotracers in chemical industry—a review, Chem. Eng. Commun. 205 (6) (2018) 739–758, https://doi.org/10.1080/00986445.2017.1410478.
[43] M.H. Lisboa, D.S. Vitorino, W.B. Delaiba, J.R.D. Finzer, M.A.S. Barrozo, A study about particle motion in rotary dryers, Braz. J. Chem. Eng. 24 (3) (2007) 365–374. https://www.scielo.br/j/bjce/a/dGNdtNDQFjKfrJ7jHRfCF4L/?lang=en.
[44] J. Thibault, P.I. Alvarez, P. Blasco, R. Veja, Modeling the mean residence time in a rotary dryer for various types of solids, Dry. Technol. 28 (10) (2010) 1136–1141, https://doi.org/10.1080/07373937.2010.483045.
[45] Miao-Ling Li, Yong-Yu Yao, Hong-Xia Zhao, Numerical analysis of solid materials transport in a rotary dryer. Advances in engineering research (AER), 105, in: 3rd Annual International Conference on Mechanics and Mechanical Engineering, MME, 2016, in: https://www.atlantis-press.com/proceedings/mme-16/25871486.
[46] M.B.A. Anuse, S.P. Chavan, Evaluation of residence time for drying of wet bagasse in A rotary bagasse dryer used in jaggery plant, Int. J. Eng. Sci. Invent. (IJESI) 7 (8) (2018) 35–41. http://www.ijesi.org/papers/Vol(7)i9/Version-3/G0709033541.pdf.
[47] C.F. Prutton, C.O. Miller, W.H. Schuette, Factors influencing rotary dryer performance, Trans. Am. Inst. Chem. Eng. 38 (1942) 251–257.
[48] W.C. Saeman, T.R. Mitchell, Analysis of rotary dryer performance, Chem. Eng. Prog. 50 (1954) 467–475.
[49] J.J. Kelly, Rotary drying, in: A.S. Mujumdar (Ed.), Handbook of Industrial Drying, Marcell Dekker Inc., New York, 1995, pp. 161–183.
[50] M.A. Karali, E. Specht, J. Mellmann, H.A. Refaey, M.R. Salem, A.Y. Elbanhawy, Granular transport through flighted rotary drums operated at optimum loading, Dry. Technol. 38 (2020) 495–505, https://doi.org/10.1080/07373937.2019.1582062.
[51] O. Levenspiel, Chemical Reaction Engineering, 3a ed., Limusa Wiley, Mexico, 2004, p. 678.
[52] C. Kreutz, K.Q. Carvalho, F.H. Passig, A.D. Belini, C.S. Cordovil, S.D. Gomes, Impact of the hydraulic loading rate on the hydrodynamic characteristics of an anaerobic fixed bed reactor treating cattle slaughterhouse wastewater, Eng. Agrícola 38 (3) (2018) 403–410, https://doi.org/10.1590/1809-4430-Eng.Agric.v38n3p403-410/2018.
[53] A.E. Rodrigues, Residence time distribution (RTD) revisited, Chem. Eng. Sci. 230 (2021), 116188, https://doi.org/10.1016/j.ces.2020.116188.
[54] A.D. Martin, G.T. Velitchko, I.R.D. Martin, D.F. Lawler, An enhanced tanks-in-series model for interpretation of tracer tests, J. Water Supply Res. Technol. - Aqua 54 (7) (2005) 435–448, https://doi.org/10.2166/aqua.2005.0041.
[55] R.E. Treybal, A.R. García, Operaciones de transferencia de masa, 2th Edition, McGRAW-HIL, 1986, p. 865. ISBN 968-6046-34-8.
[56] C. Zalazar-Oliva, E. Góngora-leyva, A.A. Legrá-Lobaina, Y.M. Retirado, J. Van Caneghem, Determinación del calor específico del mineral laterítico mediante el método de calorimetría diferencial de barrido, Miner. Geol. 37 (3) (2021) 318–332. http://scielo.sld.cu/scielo.php?script=sci_arttext&pid=S1993-80122021000300318.
[57] A.H. Pons, et al., Termodinámica técnica para ingenieros químicos, Editorial Pueblo y Educación, La Habana, 1987. SNLC:CU01.52850.5.
[58] J.H. Keenan, Steam Tables: Thermodynamic Properties of Water, Including Vapor, Liquid, and Solid Phases (English Units), 1969. ISBN 13: 9780471465003.
[59] C. Duchesne, J. Thibault, C. Bazin, Modelling and dynamic simulation of an industrial rotary dryer, Develop. Chemical Eng. Mineral Proces. J. 5 (3–4) (1997) 155–182, https://doi.org/10.1002/apj.5500050301.
[60] A. Pérez, J. Díaz, C. Guío, V. Castañeda, Efecto de la formación del manto de lodos sobre el comportamiento hidrodinámico de un reactor UASB a escala real, Revista I3+ 3 (2014) 10–29. https://revistasdigitales.uniboyaca.edu.co/index.php/reiv3/article/view/69.
[61] A.R. Vargas, A.G. Pérez, Análisis de la curva de distribución del tiempo de residencia en un Sistema de Lixiviación, Tecnol. Quím. 30 (1) (2010) 61–68, e-ISSN: 2224-6185, https://tecnologiaquimica.uo.edu.cu/index.php/tq/article/view/964.
[62] F. Cantelaube, D. Bideau, S. Roux, Kinetics of segregation of granular media in a two-dimensional rotating drum, Powder Technol. 93 (1) (1997), https://doi.org/10.1016/S0032-5910(97)03213-0.
[63] X. Liu, X. Wang, Z. Xu, T. Zou, Evolution of the driving forces during convective drying of carrot slices, J. Phys. (2018), https://doi.org/10.1088/1742-6596/1064/1/012036.
[64] O.F. Belette, Comportamiento del secado solar de lateritas a la intemperie en condiciones de clima húmedo tropical, HOLOS 7 (2020) 1–14, https://doi.org/10.15628/holos.2020.9767.
[65] S.S. Agustini, Regenerative Action of the Wall on the Heat Transfer for Directly and Indirectly Heated Rotary Kilns, Doctoral thesis, Otto-von-Guericke-Universität Magdeburg, 2006, https://opendata.uni-halle.de//handle/1981185920/10751.
[66] M.J. Moran, T.J. Higgins, Analytical heat diffusion theory,: by A. V. Luikov, J. Franklin Inst. 289 (5) (1970) 406–408, https://doi.org/10.1016/0016-0032(70)90211-5.